Full length article

Functionalization of SPION nanoparticle with malic acid for the development of superfinish optical surface

Md Amir [a], Rohit Sharma [a], Vinod Mishra [b], Kamal K. Pant [c], Amit K. Agarwal [c], Daewook Kim [d], S. Wazed Ali [e], Gufran Sayeed Khan [a],*

[a] Centre for Sensors, Instrumentation and Cyber-physical System Engineering (SeNSE), Indian Institute of Technology Delhi, Hauz Khas, New Delhi 110016, India
[b] Optical Devices and Systems, CSIR-Central Scientific Instruments Organisation, Chandigarh 160030, India
[c] Instruments Research and Development Establishment, Dehradun 248008, India
[d] Wyant College of Optical Sciences, University of Arizona, 1630 E. University Blvd., Tucson, AZ 85721, USA
[e] Department of Textile & Fibre Engineering, Indian Institute of Technology Delhi, Hauz Khas, New Delhi 110016, India

ARTICLE INFO

ABSTRACT

Optical instruments such as X-ray optics, high-power laser systems, synchrotron beamlines, lithography, and laser-based sensors, require a superfine optical surface to meet their tight optical performance tolerances. This study describes the development of a nanocomposite-based nanoabrasive that can provide a superfinish optical surface via optical polishing. The Malic acid as an organic surface modifier is functionalized with the superparamagnetic iron oxide nanoparticles (SPION). Strong chemical attachment between SPION nanoparticles and the Malic acid is verified through fourier transform infrared spectroscopy. A significant enhancement in the surface area and zeta potential value of SPION nanoparticles is observed when it is functionalized with the Malic Acid. The particle size distribution of the functionalized nanoabrasive is also narrowed down to 8–26 nm. The polishing performance of the functionalized SPION nanoabrasive has been investigated on the BK7 and Fused Silica glasses for precision optical polishing. The polishing results showed superfine surface finishing of the BK7 glass and the Fused silica glass down to the Ra value of 0.23 nm and 0.1 nm, respectively.

1. Introduction

Current technology of optical instruments such as astronomical telescopes [1], aerospace [2], synchrotron beamlines [3], navigation [4], extreme ultraviolet lithography systems [5], laser-based sensors [6], high-power lasers system [7], semiconductor materials, [8], and X-ray optics [9,10] requires high-quality optical components with superfinished Root Mean Square (RMS) surface roughness of around 1–3 Å. The application of superfinish surface and its effect on the performance of optical instruments such as X-ray optics is experimentally carried out by R. Graue et al. 1996 [11]. The developed superpolished process for X-ray Mirror reduces the high-frequency surface roughness of the Mirror and makes the surface superfinished in nature. The superfinished Mirror used for X-ray Wolter I mirror shells provides better scattering properties than the Mirror not polished by superpolished technology. Another study done by Lei Wang et al., 2006 [12]; shows the effect of surface

roughness on the measurement of a high-power laser with a cone-shaped cavity. The importance of superfinish surfaces significantly highlighted in the reported literatures. However, there are challenges to produce a high-quality surface for such applications using the conventional optical fabrication process. To obtain a superfine surface, a couple of abrasive-assisted processes have been explored, such as Magneto-Rheological Finishing [13], Ball End Magneto-Rheological Finishing [14], Abrasive Flow Finishing [15], Magnetic Abrasive Finishing [16], Magneto-rheological Abrasive Flow Finishing [17], Elastic Emission Machining [18], Magnetic Float Polishing [19], and Chemical–Mechanical Polishing (CMP) [20].

The CMP process is a conventional polishing process for optical glass and metal surfaces, and it's one of the essential fabrication steps in creating a high-quality surface. The parameters such as pressure, velocity, relative speeds between the polishing tool and workpiece, polishing time, and well-conformed polishing pads [21,22] are crucial for

---

the CMP process to achieve high-quality surface. However, to achieve superfinished surface via chemical induced mechanical process, certain properties of the abrasive materials need to be altered to get a homogenous nanometric cutting effect along with angstrom level surface finishing. Nanoparticles are suitable candidates for such operation as they have a large surface area (in terms of surface to volume ratio), allowing homogeneous shearing and faster material removal which improves the smoothness of the desired optical surfaces. The particle size distribution of the abrasive and its colloidal effect also plays an important role during polishing and their impact on polishing efficiency [23–25]. Conventional abrasive possesses large particles of low surface area and have a wide range of particle size distribution which hinder the CMP performance for superfinish surface manufacturing [26,27].

Recently we have developed a nanoabrasive based on pure SPION magnetic nanoparticles [28]. This magnetic nanoabrasive showed enhanced CMP performance for superfinish optical surfaces. Magnetic nanoparticle-based polishing abrasives are useful in creating eco-friendly and pollution-free materials [29]. Their unique separation technique helps users to recycle and reuse the used materials with the help of an external magnetic field [30]. The utilization of magnetic nanoparticle-based polishing abrasives can help to reduce the million tons of wasted abrasives that throw into the garbage without reutilization [31]. The polishing abrasives based on nanoparticles have a high probability of agglomeration, thus increasing particle size distribution. Agglomeration and wider particle size distribution reduce the overall material removal rate and the contact area between the workpieces. As a result, polishing efficiency decreases.

The optimized particle size distribution of 10–60 nm of the bare SPION-based nanoabrasive is developed along with a low surface area of $30.98 \text{ m}^2\text{g}^{-1}$ and it is reported in our previous study. Therefore, SPION-based nanoabrasive has a limitation to achieve the surface roughness (Ra) lower than 0.2 nm, which led to the need for the functionalization of SPION nanoparticle with a specific surface modifier. A surface modifier can help in achieving a narrow particle size distribution along with a high surface area by reducing the agglomeration effect [32,33].

This study reports the development of a magnetic nanocomposite-based polishing abrasive which can have a very narrow particle size distribution, high surface area, and can provide a superfinish surface of low surface roughness of few Angstroms (1–3 Å or 0.1–0.3 nm). The Malic acid as surface modifier is functionalized with SPION magnetic nanoparticle via a modified hydrothermal route. The developed nanocomposite-based nanoabrasive is explored on both the BK7 and Fused silica optical glasses, which are the two widely used glass types in precision optical manufacturing, for super smooth polishing. It also showed superparamagnetic properties with a low value of remanent magnetization and magnetic coercivity. This superparamagnetic nature acts as a magnetic core that assists in recycling the used nanoabrasives via magnetic separation.

2. Preparation and characterization

2.1. Preparation of the functionalized nanoabrasive

The SPION nanoparticle was functionalized with a surface modifier such as Malic acid via a modified hydrothermal route. Cost-effective Iron salts precursor of Ferrous sulphate heptahydrate, 99.5 % ($FeSO_4 \cdot 7H_2O$) from CDH chemical, Ferric chloride hexahydrate 99.00 % ($FeCl_3 \cdot 6H_2O$), and Malic acid ($C_4H_6O_5$) from Merck were mixed with the double distilled water in a molar ratio of 1:2:0.0007:4.4. Thereafter, the pH of the dispersion was controlled to 7 by adding 0.09 M of sodium hydroxide (NaOH). The colour of the dispersion turned black from brown on the addition of an alkaline solution. This indicates the formation of functionalized SPION-base nanocomposites. To control the morphology and particle size distribution, the produced black hydrated powder was transferred to a stainless-steel autoclave and placed in a heating oven at 150 °C for 18 hours. The resultant product was collected by a magnetic

separation process. The separated hydrated powder is then rinsed in ethanol before being dried in a heating oven for 8 hours at 90 °C. Complete synthesis process has been schematically shown in Fig. 1.

2.2. Characterization of the functionalized nanoabrasive

The X-ray diffraction powder patterns of the functionalized nanoabrasives are depicted in Fig. 2a. The observed peaks indicate the polycrystalline nature and the phase information of the final products of the Malic acid-functionalized SPION nanoabrasive. The characteristic diffraction peaks for the nanoabrasive appeared at diffraction angle (2θ) values of 18.65°, 30.18°, 35.63°, 37.86°, 43.17°, 45.08°, 53.68°, 57.37°, 62.98°, and 74.01° which correspond to hkl planes of (1 1 1), (2 2 0), (3 1 1), (2 2 2), (4 0 0), (1 1 0), (4 2 2), (5 1 1), and (4 4 0), respectively [34], and are matched with standard JCPDS card No.19–629 of SPION.

Fig. 2b shows the infrared spectra of a bare malic acid and its functionalized nanoabrasive, respectively. Two low-frequency vibrational stretching of metal–oxygen (Fe—O) bond interactions are observed at the absorption band of 456 cm^{-1} and 558 cm^{-1} confirming the presence of SPION particles [35,36]. The symmetric and asymmetric vibrational stretching frequencies of the —OOC carboxylic group of the surface modifier are observed at 1687 cm^{-1} and 1463 cm^{-1} [37] as shown in Fig. 2b. The chemical binding of the malic acid with the SPION surface disturbed the symmetric and asymmetric vibrational stretching frequencies of the O=C=O of the Malic acid to 1622 cm^{-1} and 1402 cm^{-1} in the FTIR spectra of the functionalized nanocomposites as shown in Fig. 2c. This covalent interaction is caused by the hydrogen bonds between the surface modifier and the SPION particles [34]. At the broad vibrational frequency range of 2800–3280 cm^{-1}, a hydroxyl (—OH) adsorption of Malic acid is observed.

Transmission electron microscopy (TEM) micrograph and particle size distribution analysis of the Malic acid-functionalized SPION nanocomposites-based nanoabrasive are presented in Fig. 2d and 2e, respectively. The morphology of the prepared nanoabrasive is observed as spherical in shape. The particle size can be seen in nanosize with less agglomeration. This insignificant agglomeration is due to the higher surface energy of smaller particles, surface charge interaction, and magnetic property of the SPION particle. The particle size distribution of the developed nanoabrasives is estimated within the narrow range of 8–26 nm.

The effect of the Malic acid functionalization with the SPION and its effect on the surface area of the overall nanoabrasive are investigated by the Brunauer-Emmet-Teller method. It is widely used to evaluate the surface area, pore size, total pore volume, adsorption, and desorption capabilities of the resultant material. The BET adsorption/sorption curve is classified into four isotherms [38,39]. The functionalized nanocomposites-based nanoabrasives have a Type IV isotherm with a hysteresis loop, as shown in Fig. 2f. The surface area of the prepared nanoabrasives has been estimated as 54.38 m^2/g. A large pore diameter of 16.48 nm has been calculated by the Barret-Joyner-Halenda method. The estimated surface area and pore diameter of the developed magnetic nanocomposites-based nanoabrasive suggest an enrichment of active sites for adsorption. It also implies a broad surface area on the vapor adsorbate with a uniform particle dispersion. The predicted characteristics promote significant enhancement in homogeneous/stable material removal and strong particle adsorption compared to the pure SPION nanoabrasive case as shown in Table 1.

3. Magnetic property and recovering test of malic acid-functionalized SPION nanoabrasive

The developed Malic acid functionalized SPION nanoabrasive's magnetic coercivity (H) and hysteresis (r) values are studied using the physical properties measurement system (PPMS) technique. The magnetic flux value of the functionalized magnetic nanocomposite-based nanoabrasive has been determined by (M−H curve which is also
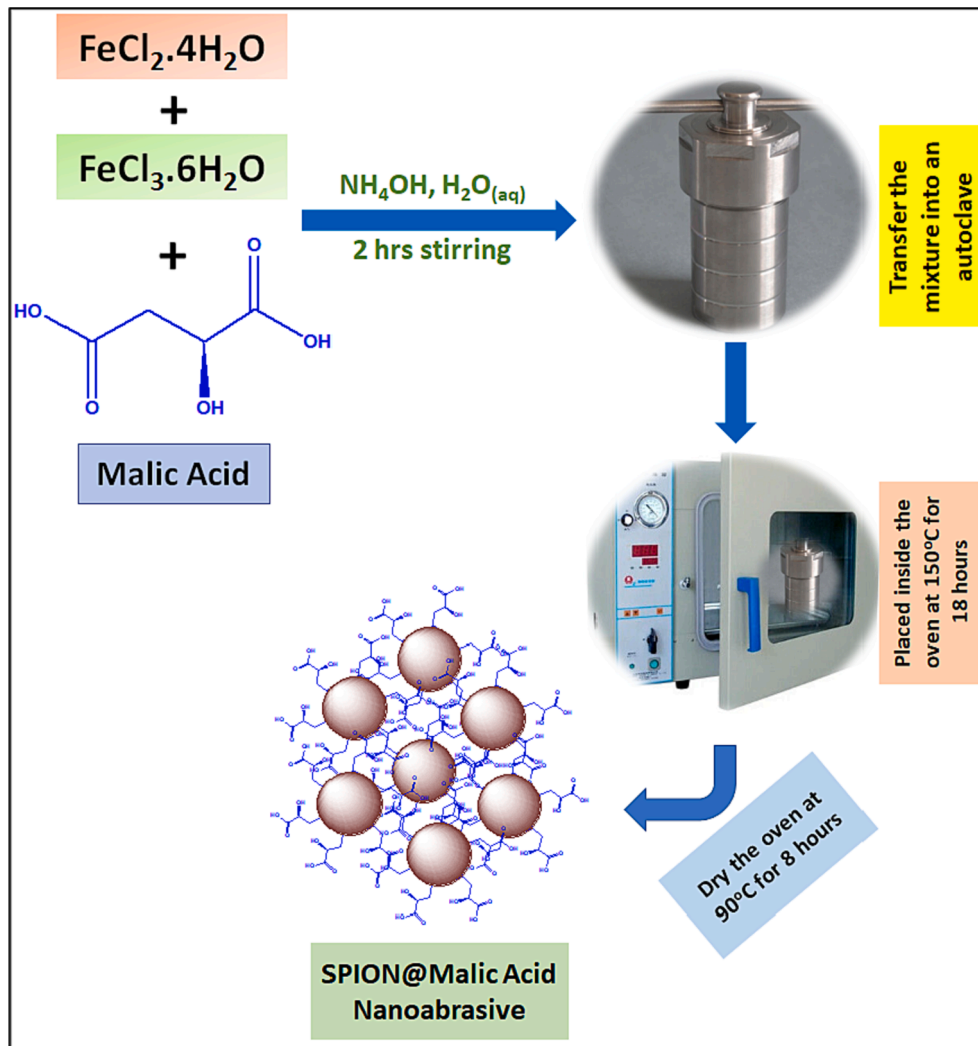
Fig. 1. Synthesis route of the Malic acid-functionalized SPION nanocomposite-based nanoabrasive.

known as the magnetic hysteresis curve where M and H represent the magnetization and measured magnetic field, respectively [40]. The magnetic measurement was done under the varying magnetic field of $+$1,000 A/m to $-$1,000 A/m up to 10 KOe as illustrated in Fig. 3a. The measured M−H hysteresis curve of the Malic acid functionalized SPION-based nanoabrasive gives a maximum magnetization (σ) value of 53.8 emu/g. The measured value of "σ" correspond to H = 10 KOe is not saturation magnetization (σ_s). To further examine the value of "σ_s", a well-established Wohlfarth (S–W) mathematical model for magnetic saturation was introduced [41,42]. As per the S-W model, the plot between σ against $1/H^2$ provides the saturation magnetization values if it is close to zero. The σ versus $1/H^2$ graphs for the functionalized nanocomposites-based nanoabrasive is shown in Fig. 3b. The magnitude of "σ_s", is determined to be 54.32 emu/g for the Malic acid functionalized SPION-based nanoabrasive. The estimated saturation magnetization value of the synthesized nanoabrasive is lesser than the saturation magnetization values of pristine SPION [43–45]. There are distinct reasons for getting lower magnetization values of functionalized SPION nanocomposites, and concisely it is because of the capping of diamagnetic material such as Malic acid on the surface of tiny SPION particles [46]. Another reason that could be responsible for lowering the magnetization values of the overall nanocomposites-based nanoabrasive is distortion in the surface spin of antiferromagnetic interactions as hypothesized by J.M.D. Coey [47]. Further investigation on the magnetic property of the synthesized Malic acid-functionalized SPION-based

nanoabrasive was done.The coercivity (H) and magnetic remanence (σ_r) values were extracted from M−H curves, and related results are provided in Table 2. The low H and σ_r values indicate the superparamagnetic nature of the prepared functionalized nanoabrasives as observed by a couple of researchers [48,49]. This superparamagnetic nature helps the users extract the used abrasives from the aqueous slurry with the help of an external magnetic field. The separated abrasive can be recycled and reused after a cycle of optical polishing.

4. Zeta potential of the slurries

Zeta potential measurement of the aqueous slurries based on the developed Malic acid functionalized SPION nanoabrasive at different pH has been investigated via the dynamic light scattering technique. Fig. 4 presents the effect of pH on the zeta potential of the prepared Malic acid-functionalized SPION nanoabrasive-based slurries. The highest zeta potential of –32.4 mV is measured for the functionalized-nanoabrasive-based aqueous slurry at a high pH of 12. As the pH value increases, the zeta potential also increases. The addition of a few drops of highly alkaline solution stabilized the zeta potential of the prepared slurry. After introducing an alkaline solution, a substantial quantity of —OH molecules are adsorbed on the surface of Malic acid-functionalized SPION particles. The adsorption property of SPION which is a metal oxide material is a variable of pH values [50]. The variable charges of the oxide and hydroxide become more negatively charged when pH
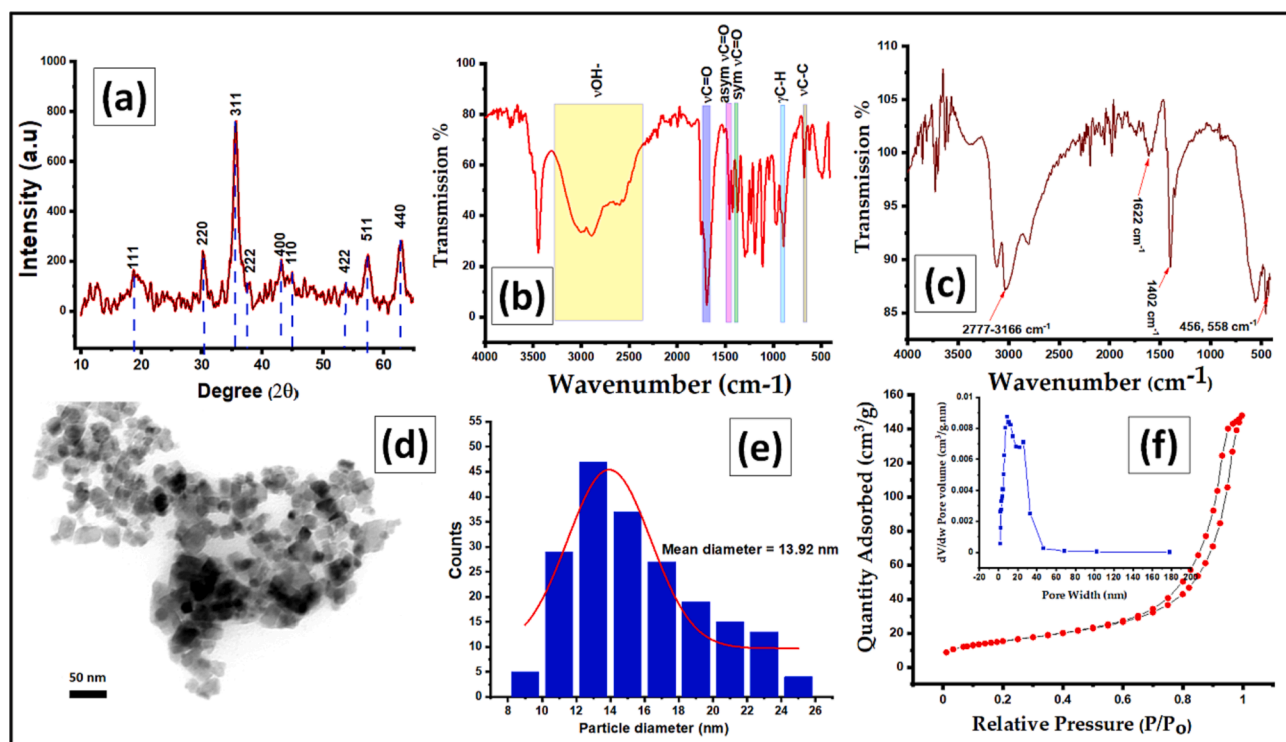
Fig. 2. (a) XRD powder pattern, (b) FT-IR spectra of pure-Malic acid molecules, and (c) Malic acid-functionalized nanocomposite-based nanoabrasive, (d) TEM micrograph, (e) particle size distribution curve and (f) BET surface area and pore volume curves (inset) of the Malic acid-functionalized SPION-nanocomposite-based nanoabrasive.

Table 1
Particle size and surface area of the developed Malic acid-functionalized SPION nanoabrasive in comparison to pure SPION nanoabrasive.

Nanoabrasive	Average particle size (nm)	Particle size distribution (nm)	BET surface area (m²g⁻¹)	Pore size (nm)	Ref.
SPION	34.90	10–60	30.98	6.13	[26]
SPION@Malic acid	13.92	8–26	54.38	16.48	Present study

values get high and allow surface hydroxy groups that lose protons to adsorb the metal ions more easily from the aqueous solution [51]. When an acid is added to the water, it increases the concentration of H_3O^+ ion; similarly when a base is added to the water, it elevated the concentration

of OH^- ion. This can be understood better with the following reaction.

$$NH_3 + H_2O \longleftrightarrow (NH_4)^+ + OH^- \tag{1}$$

When ammonia is added to the slurry made up of SPION, which is one of the kinds of metal oxide, the water molecules that lose protons, possess large numbers of hydroxy groups that comes from added alkaline ammonia solution and they adsorb onto the surface of SPION. The experimental IR-spectrum of pH dependent aqueous slurry of SPION is given in Fig. 4c. It can be observed that the absorption concentration of —OH at a broad vibrational stretching of 3250–3357 cm⁻¹ is higher for higher pH containing slurry. The absorption peak at 1622 cm⁻¹ corresponds to the symmetric vibrational stretching frequency of the —OOC carboxylic group of the malic acid attached to surface of SPION and confirmed from FTIR results in Section 2.2. Therefore, the adsorption of hydroxyl (OH⁻) on SPION@Malic acid nanoabrasives particles' surfaces
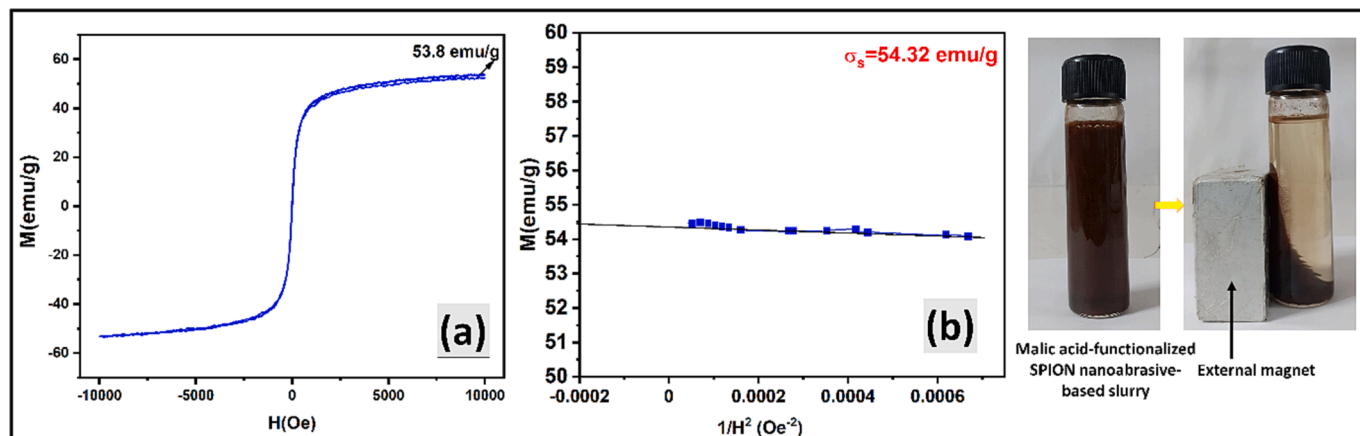
Fig. 3. (a) M−H hysteresis curve and **(b)** plots of σ vs 1/H² for Malic acid-functionalized nanoabrasive at room temperature.

Table 2

Magnetic properties of developed Malic acid-functionalized SPION nanoabrasive in comparison to pure SPION nanoabrasive.

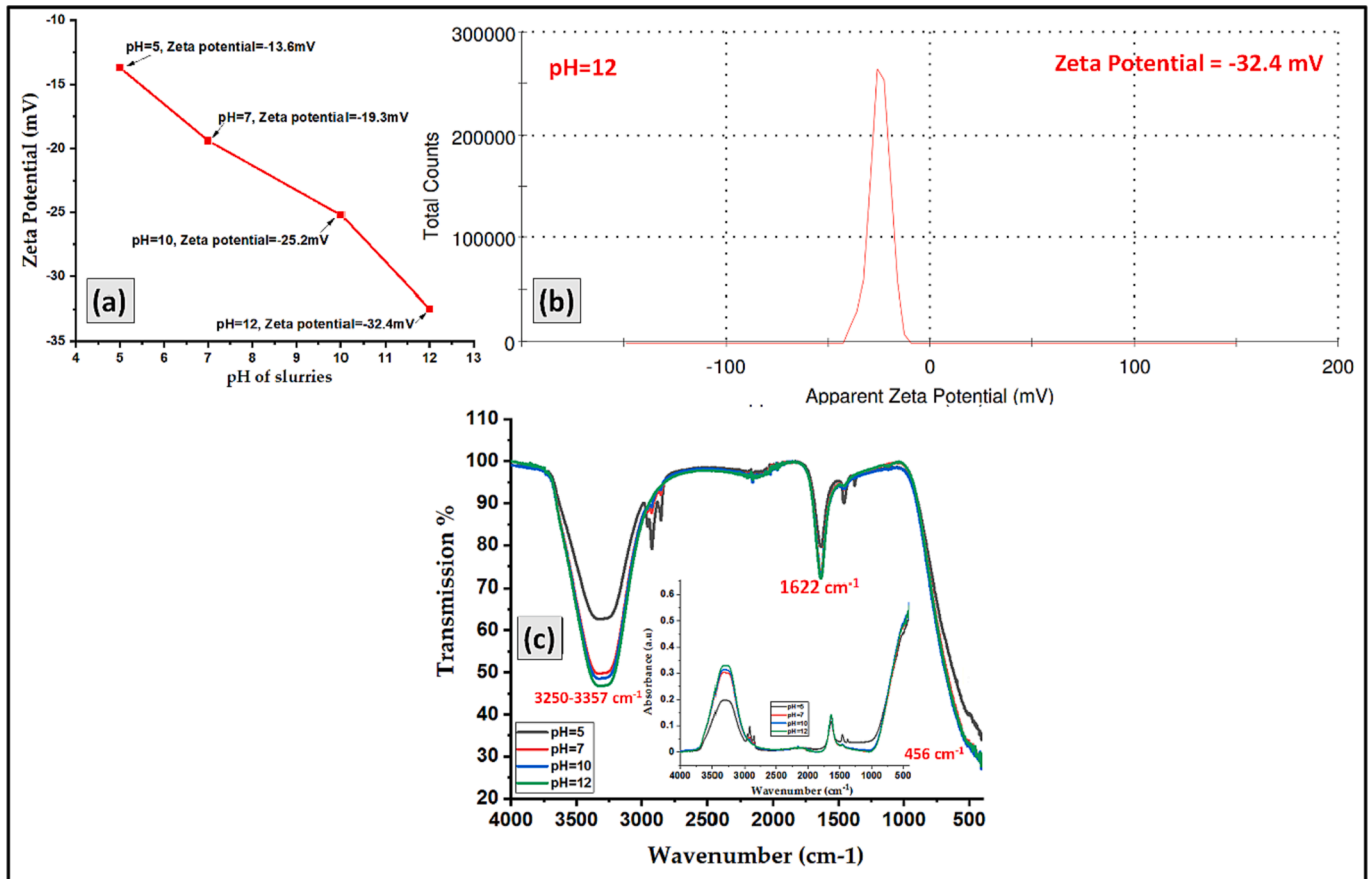| Nanoabrasive	Magnetization, σ (emu/g)	Saturation magnetization, σ_s (em/g)	Coercivity, H (Oe)	Magnetic remanence, σ_r (emu/g)	σ_r/σ_s	Ref.
SPION	66.65	68.52	10.8	2.64	0.0385	[26]
SPION@Malic acid	53.80	54.32	5.68	1.2	0.0220	Present study

Fig. 4. (a) Zeta potential variation concerning pH of Malic acid-functionalized SPION nanoabrasive-based polishing slurries, (b) Zeta potential of slurry at pH = 12, and (c) effect the pH on the adsorption of SPION via IR spectrum.

creates negatively charged electric double layers. This improves the suspension stability, resulting in a high negative zeta potential value.

A repulsion force is also acted between the nanoabrasive particles due to the same charge, resulting in the deagglomeration of nanoabrasive. This increases the surface area and even dispersion of particles on the glass's surface. In a typical mechanically driven chemical mechanical polishing process, interactions between the abrasive particles and the upper layer of the optical glass specimen which constitute of Si-O layers play a crucial role. The pH of the colloidal slurry and its surface charges can alter this interaction [52]. The slurry's high hydroxyl radical is the pre-requirement for enhancing the chemical interaction between the abrasive particle surface and the workpiece's top surface, resulting in a high material removal [53,54].

5. Experimental performance of the malic acid-functionalized SPION nanoabrasive-based slurries

A BK7 glass disc (50 mm diameter and 6 mm thickness) and a fused silica glass disc (45 mm diameter and 8 mm thickness) are taken to perform the experimental CMP process investigation. The specimens are pre-processed by conventional coarse/fine grinding and roughing steps. The obtained surface roughness after conventional roughing is to a few hundreds of nanometres. Colloidal slurries of the developed Malic acid-

functionalized SPION nanocomposite-based nanoabrasives are prepared with double-distilled water at three different pH values with 5 % concentration. The CMP process is carried out with a 0.5 mm thick Polyurethane pad (LP-66) and a pitch (resin-based) polisher separately, using polishing equipment (LOHTRONIC, Model HLP 150–4). The CMP process with pitch and pad laps is done on a flat surface with a regulated spindle speed and stroke, resulting in a completely controlled polishing motion. The polishing condition has been set at a downforce as shown in Fig. 5, adjusted by the physical weight setting on the machine under the pad rotation of 80 rpm. The slurry is supplied manually with the help of a polymer dropper. Each iteration of the polishing experiment of different batches by varying the pH of the colloidal slurries is performed under control working environment such as temperature, and humidity of the polishing area and it was maintained same for all the batches of the polishing experiment. The specimens are cleaned with 99.99 % acetone after the final iteration. The surface roughness improvement has been investigated by CCI after each 30 min duration.
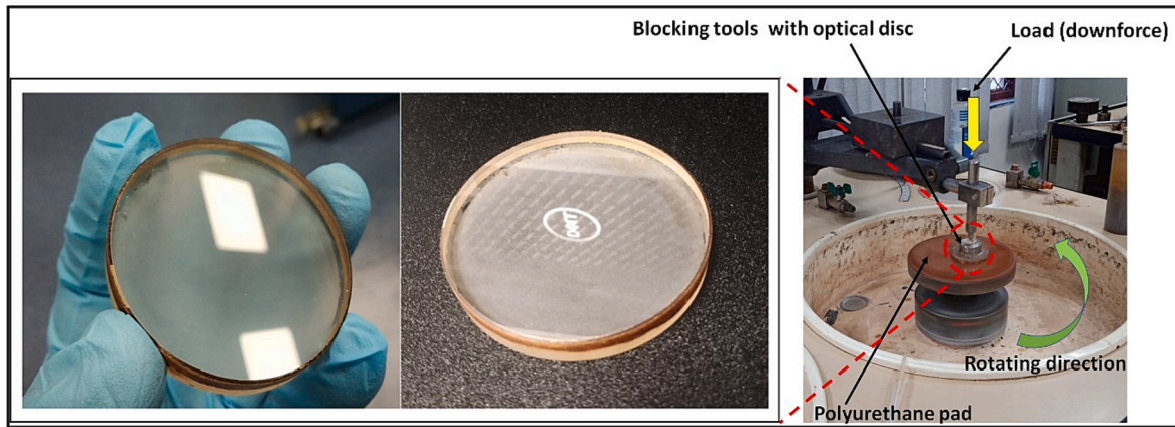
Fig. 5. The schematic representation of the CMP process of fused-silica glass on a polyurethane pad with the developed Malic acid-functionalized SPION nanoabrasive-based slurry. The schematic is the same when pitch polisher is used.

5.1. Polishing performance of functionalized SPION nanocomposite-based nanoabrasives

5.1.1. BK7 pad polishing with functionalized SPION nanoabrasives-based slurries

The polishing performance of the Malic acid-functionalized SPION nanoabrasives-based colloidal slurry is demonstrated and verified first on a BK7 glass disc, which is one of the most commonly used glass materials in the optical manufacturing community. The main goal of this study is to investigate the effects of the pH of the slurry on the polishing performance of the glass specimen. For pH-based polishing, three different colloidal slurries of 5 % concentration by weight/volume of the developed nanoabrasives at three different pH of 5, 7, and 12 have been prepared.

The polishing results in terms of area surface roughness (Sa), and surface roughness (Ra) are presented in Fig. 6. The initial Ra of a pre-polished BK7 glass disc is measured as 240.3 nm. It is reduced to a Ra value of 16.9 nm after 120 min of the polishing using the prepared colloidal slurry of Malic acid-functionalized SPION nanoabrasives at a pH of 5. Similar trend has been observed for the prepared colloidal slurry at pH of 7 and 12, yet the surface of the BK7 disc is still very rough. However, a notable improvement in the surface quality of the disc is observed when polishing is continued further from 120 min using the developed nanoabrasives-based colloidal slurries. At the final stage, Ra lowered down to 0.54 nm. When this polishing process is repeated for higher pH of 7 and 12, the surface roughness improvement is much better than the lower pH-containing slurries. In these cases, the surface roughness improved to 0.33 nm and 0.23 nm for pH 7 and 12, respectively. This demonstrates the capabilities of the prepared colloidal slurry of Malic acid-functionalized SPION nanoabrasives in order to achieve surface roughness of couple of Angstroms.

The comprehensive polishing results at different pH and times have been provided in detail in supplementary Figs. S1-S6. The surface quality of the BK7 glass disc after the polishing is also characterized by Atomic Force Microscopy (AFM) as shown in Fig. 7. It is noticed that the Sa of the BK7 glass at high pH of 12, gets improves to 0.76 nm.

5.1.2. Fused silica pad polishing with functionalized SPION nanoabrasives-based slurries

Once it is established that at high pH value of the developed Malic acid-functionalized SPION nanoabrasives-based slurry provides much better surface finishing than the lower pH containing slurry, the polishing performance of the developed nanoabrasives is again evaluated for fused silica glass disc of 45 mm in diameter and 8 mm in thickness as fused silica is widely used in the applications where superfinish and high material purity is one of the necessities.

The pH of the prepared nanocomposites-based colloidal slurry of 5 % concentration is maintained to 12. Fig. 8 shows the polishing results of the pre-polished and polished fused silica surface in terms of Ra and Sa. The Ra of a pre-polished fused-silica glass disc is found as 397 nm. It is lowered down to a Ra value of 30.4 nm after 30 min of the polishing using the colloidal slurry of Malic acid-functionalized SPION nanoabrasives. A significant improvement in the surface quality of the fused-silica disc is observed after 120 min of polishing and the Ra is reduced to 0.7 nm. The detailed experimental results of the surface quality improvement with respect to time in terms of Ra are provided in supplementary Fig. S7.

At the final iteration of the CMP of fused-silica glass disc using the prepared malic acid-functionalized SPION nanoabrasives-based slurry, the surface roughness is reduced to 0.1 nm, and it is presented in Fig. 8d. It is noticed that the developed Malic acid-functionalized SPION nanoabrasives-based slurry is more efficient for fused-silica glass as compared to the BK7 glass for achieving a superfine surface. In both BK7 and fused-silica glass, the resulting pad-based polishing performance of the developed nanoabrasives-based colloidal slurries is suitable for maintaining high material removal.

5.1.3. Fused silica pitch polishing with functionalized SPION nanoabrasives-based slurries

A pitch polishing, which is a traditionally well-known process creating high smoothness surfaces, the experiment is performed in the same polishing conditions to compare the two approaches using the prepared colloidal slurry of Malic acid-functionalized SPION nanoabrasives to obtain a superfinish surface. A fused silica flat-circular disc of 45 mm in diameter and 8 mm in thickness, which has an initial surface roughness of 342 nm, is taken as a specimen for CMP polishing.

Fig. 9 depicts the polishing results of the pre-polished and polished fused silica surfaces in terms of Ra and Sa. As the first cycle of polishing lasted for two hours, the surface roughness of the fused-silica specimen went down to 15 nm from 342 nm. After the second iteration of polishing, the surface quality of the fused-silica disc significantly improved, and the Ra is reduced to 1 nm. The polishing is carried out for a couple of hours to make the surface super smooth. The surface finishing of the fused-silica glass disc is measured, and the Ra lower down to 0.1 nm.

6. Discussion on functionalised SPION based polishing mechanism

The material removal mechanism of the CMP process is not fully established that how different process parameters affect the material removal rate and the resulting surface topography. Various models are reported with emphasis on the mechanical aspects of CMP process such
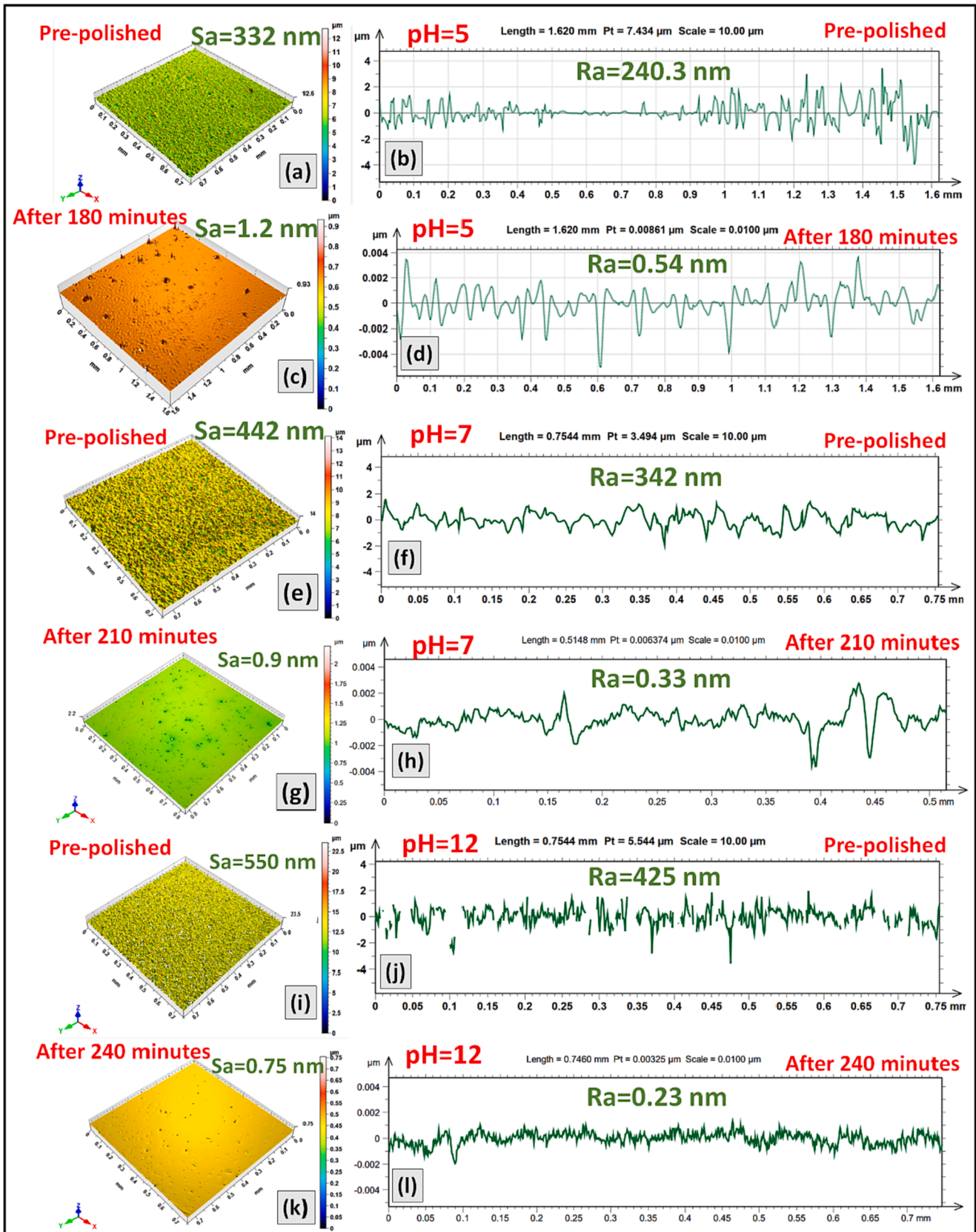
Fig. 6. Sa and Ra measurement of pre-polished and final polished BK7 glass discs using Malic acid-functionalized SPION nanocomposites-based slurry at different pH of (a-d) pH = 5, (e-h) pH = 7, and (i-l) pH = 12.
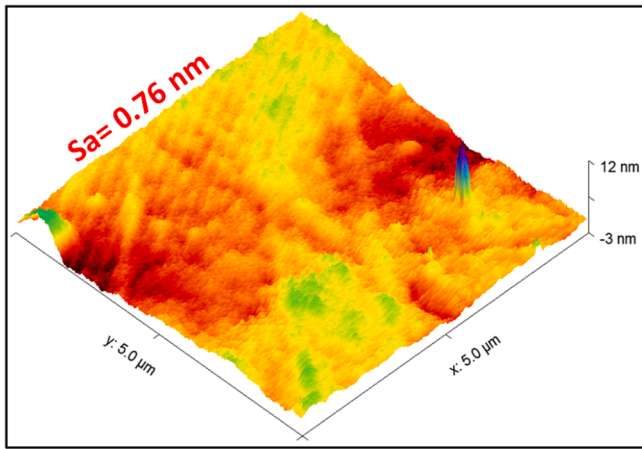
Fig. 7. Surface roughness measurement and polishing performance of developed Malic acid-functionalized SPION nanoabrasives on BK7 optical glass using AFM after final polishing.

as Sundararajan et al., 1999 [55], Liu et al., 1996 [56], Runnels and Eyman, 1994 [57], Yu, 1993 [58], and Brown et al., 1981 [59]. This study also describes the materials removal in terms of size distribution of abrasive particles, end functional group of the surface modifier, the slurry concentration, and the pH of the slurry which are considered important elements that influence the material removal capability of polishing abrasive. These parameters are principally responsible for the Malic acid-functionalized SPION nanoabrasives-based slurry's ability to reduce the glass discs' surface roughness to the sub-nanometer region. When larger particles are utilized, the material removal mechanism

during CMP generally increases. However, a smaller particle of large surface area and narrow particle size distribution under similar CMP conditions provides uniform and high material removal. This can be explained by a well-established surface area-based model [60] that describes the polishing rate in terms of particle diameter and the slurry concentration, and it is followed as:

$$A \propto C_0^{\frac{1}{3}} . \Phi^{-\frac{1}{3}} \pi \qquad (2)$$

where "A" is the total contact area between abrasive and glass substrate, "C_0" is the concentration of slurry, and "Φ" is the diameter of slurry particles. The functionalized SPION nanoabrasives possess a smaller particle size distribution (8–26 nm) as confirmed by particle size distribution analysis in Section 2.2.2 and high surface area depicted from BET analysis in Section 2.2.3. The polishing efficiency of the prepared nanoabrasives in terms of material removal is significantly high, indicating that the Malic acid-functionalized SPION nanoabrasives follow the contact area model. The small particles with narrow size distribution and high surface area, providing more contact area to the workpiece surfaces and polishers, are the cause for faster polishing with the developed nanoabrasive and this can be verified from a similar kind of material removal mechanical mechanism [61]. Additionally, the homogeneous particle distribution and low degree of agglomeration offer uniform cutting impact and accelerate the mechanically induced chemical process in CMP process.

The chemo-mechanical process for the Malic acid-functionalized SPION nanoabrasives is investigated in terms of chemical interactions between particle surface and glass surface's upper layer. Fig. 10 shows a schematic of the mechanics of the chemical mechanical polishing process using the Malic acid-functionalized SPION nanoabrasives. During the CMP process, the newly prepared nanoabrasive's aqueous slurry is hydrolysed and transformed to SPION@Malic acid(OH)$_3$. On the surface

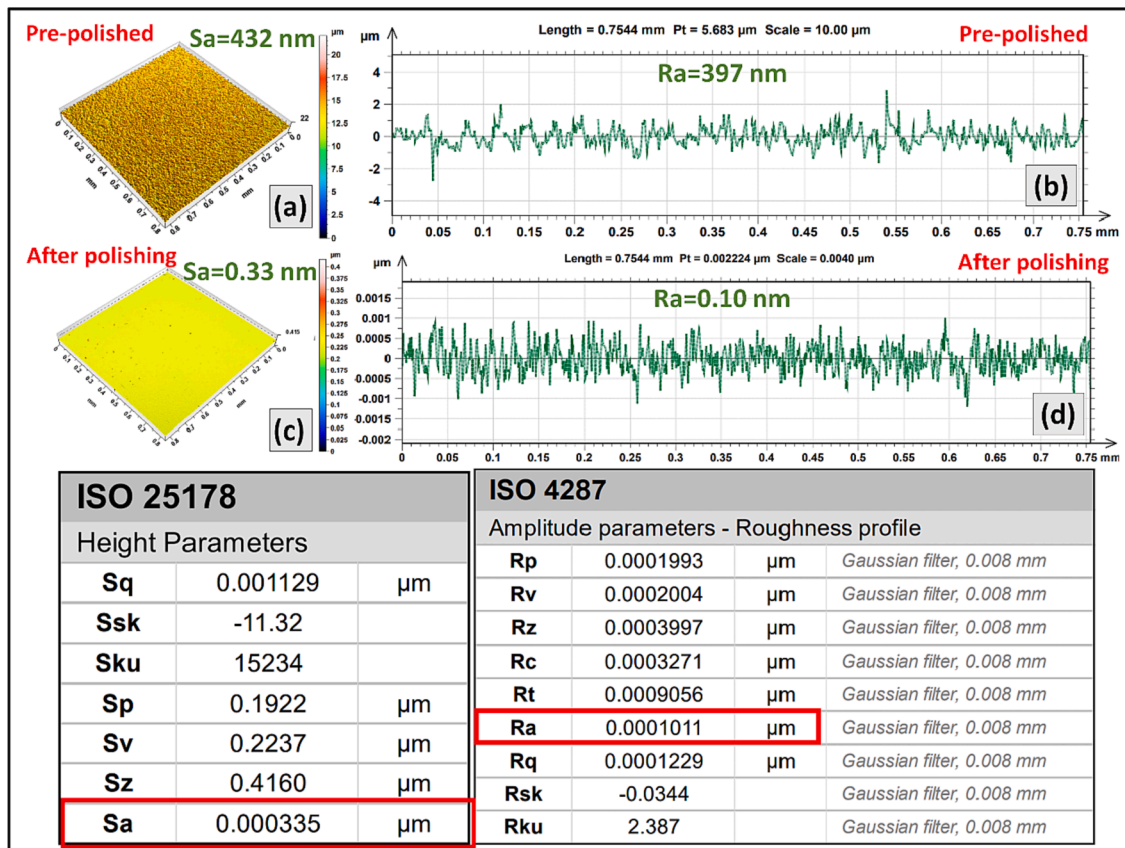| ISO 25178				ISO 4287			
Height Parameters				**Amplitude parameters - Roughness profile**			
Sq	0.001129	μm		**Rp**	0.0001993	μm	Gaussian filter, 0.008 mm
Ssk	-11.32			**Rv**	0.0002004	μm	Gaussian filter, 0.008 mm
Sku	15234			**Rz**	0.0003997	μm	Gaussian filter, 0.008 mm
Sp	0.1922	μm		**Rc**	0.0003271	μm	Gaussian filter, 0.008 mm
Sv	0.2237	μm		**Rt**	0.0009056	μm	Gaussian filter, 0.008 mm
Sz	0.4160	μm		**Ra**	0.0001011	μm	Gaussian filter, 0.008 mm
Sa	0.000335	μm		**Rq**	0.0001229	μm	Gaussian filter, 0.008 mm
				Rsk	-0.0344		Gaussian filter, 0.008 mm
				Rku	2.387		Gaussian filter, 0.008 mm

Fig. 8. Sa and Ra measurement of (a-b) pre-polished surface and (c-d) polished fused silica glass disc using the Malic acid-functionalized SPION nanocomposites-based slurry at pH = 12 via pad-based polishing.
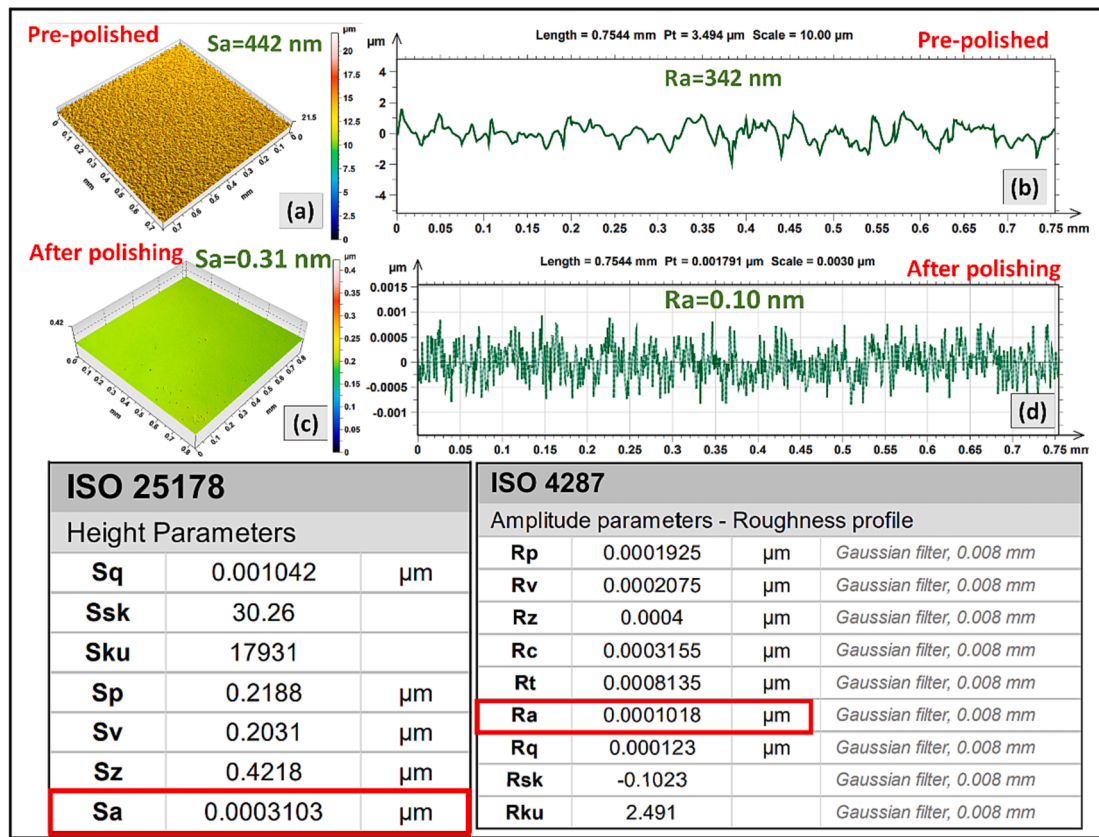
Fig. 9. Sa and Ra measurement of (a-b) pre-polished surface and (c-d) polished fused silica glass samples, respectively, using Malic acid-functionalized SPION nanocomposites-based slurry at pH = 12 via pitch-based polishing.

of the nanoabrasive particles, many —OH groups from water molecules are adsorbed. The upper layers of the workpiece have a significant amount of internal bond in the form of Si—O—Si. These SiO_2 molecules of the workpiece surface are dissolved into $Si(OH)_4$ by the hydrated SPION@Malic acid$(OH)_3$ molecules (schematically shown in Fig. 10). Similar kind of material removal was reported by L.M. Cook. [62], who proposed the interaction of both glass surface and the polishing particle such as CeO_2 in aqueous media. The interaction of the of silicate (Si-O-Si) with the water is subjected to the reversible depolymerization reaction which controls the removal rate in CMP [63]. The reversible depolymerization reaction is given below.

$$\equiv Si - O - Si \equiv + H_2O \leftrightarrow 2 \equiv Si - OH \tag{3}$$

The reversal reaction of eq. (3) is the breakage of network forming siloxane bonds by hydroxyl to form a hydrated silica surface. Such interaction is also confirmed in this study with the developed Malic acid functionalized SPION-based slurry and upper surface layer of the glass substrate. An in-situ infrared measurement was done in real time CMP polishing before the addition of aqueous slurry and during the CMP process using the aqueous slurry-based on the developed functionalized nanoabrasive and the results are presented in supplementary Fig. S8(a-b). In-situ IR spectroscopy measurement is done to identify the changes in chemical shifting of the vibrational stretching of the desired materials in real time reaction or analysis at room-temperature. The IR spectra of the glass substrate before and during CMP polishing provide number of chemical shifting of subjected functional group's interactions such as Si-O-Si bond and SPION-OH. In Fig. S8a, the vibrational stretching of —OH related to water molecules is observed at a broad band of 3035–3300 cm^{-1}. The peak at 1631 cm^{-1} corresponds to the —OH vibrations come from water and adsorbed on the surface of silica of the glass substrate in the form of Si-OH. In Fig. S8b, few new peaks such as Fe—O—Si, Fe—O, C—OH, and C=O were observed at 637 cm^{-1}, 954 cm^{-1}, 1165 cm^{-1},

and 1466 cm^{-1}, respectively due to the chemical interaction of glass surface with the aqueous Malic acid functionalized SPION-based slurry. Two sharp —OH vibrational stretching frequencies due to water molecules and hydrated glass surface are also observed simultaneously at 3391 cm^{-1} and 1632 cm^{-1}, respectively. Thus, this proved that the partial interaction between the glass and the slurry has taken place during CMP polishing and this interaction is reversible. The presence of —OH layers on SiO_2's Si—O—Si bonds affects the mechanical stability of the Si—O—Si bonds as proposed by Jianfeng's chemo-mechanical model [64]. The mathematical model proposed by Jianfeng et al., reflects the effect of the chemical action on the material removal via mechanical abrasion. The mechanical hardness and the density of the substrate are affected by the chemical action of the CMP and primarily responsible for softening the upper surface layer of the substrate to be polished. The fitting parameters of the model was unable to measure the real magnitude of the hardness and its direct effect in real time CMP polishing as it involves with interactions between chemical removal and mechanical removal. The mechanical hardness of the softened hydrated layer of the substrate due to the chemical action of the CMP is different than that actual mechanical hardness of the substrate material as per the model. With low mechanical hardness, it becomes gelatine in nature. Heat is generated on the glass surface during polishing due to the mechanical friction in the CMP process, which provides energy to weaken the Si–O–Si bonds. The magnitude of the heat generated, and the mechanical hardness softened due to mechanical and chemical action, respectively could not be measured by Jianfeng's chemo-mechanical model in real time CMP polishing and still subject of considerable debate [65]. The weakly bounded molecules removed into very small-size chips through a mechanical action of the CMP. The removal chips of the glass substrates during CMP along with the used slurry were recovered and it was analzyed by high-resolution scanning electron microscope and energy dispersive X-ray technique as shown in Fig. S8(c) and Fig. S8(d),
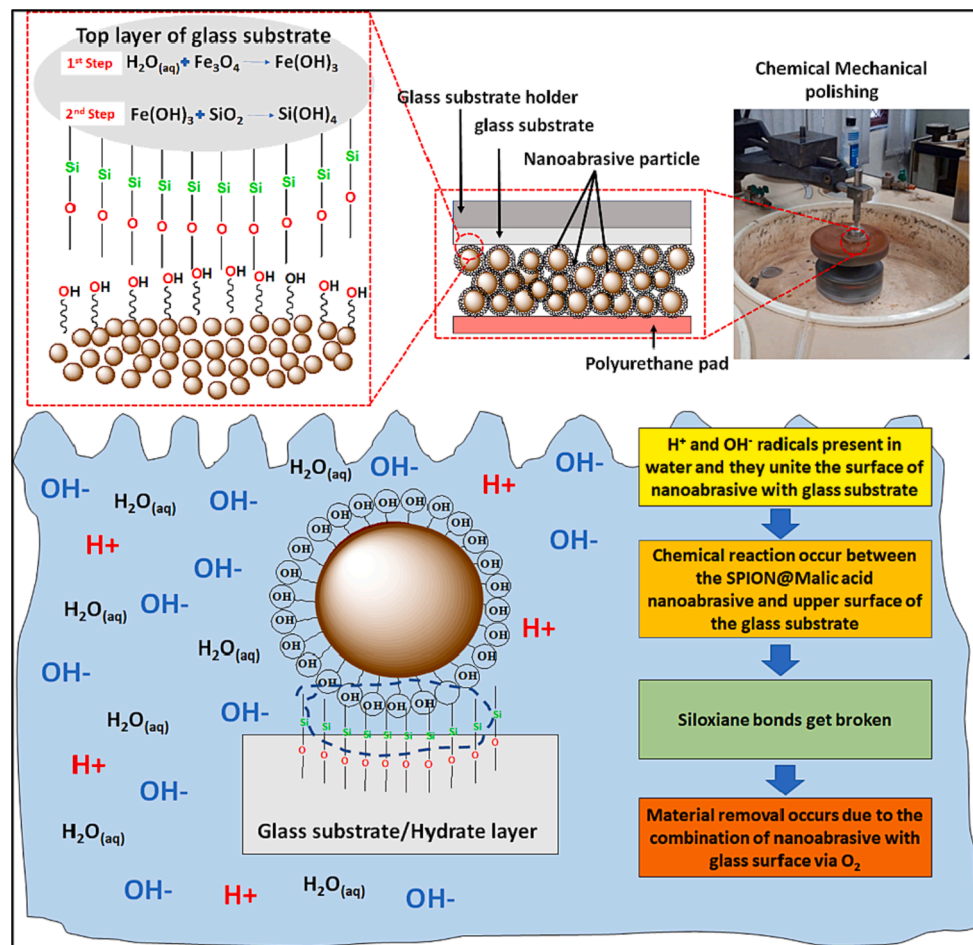
Fig. 10. The schematic of the polishing mechanism for developed Malic acid-functionalized SPION nanoabrasives-based slurry.

respectively. It can be seen in the Fig. 8S(c) that glass chips which were removed by mechanical action of the CMP are in micro and nano size. The height of irregularity peaks continues to decline, resulting in improved surface finishing. Therefore, the developed Malic acid-functionalized SPION nanoabrasives provide a higher material removal and a superfine finishing process for both the glass specimens. It's also been discovered that increasing the pH of the prepared slurry promotes the synthesis of $Si(OH)_4$ molecules more faster during polishing, which speeds up the Malic-acid functionalized SPION nanoabrasives-based slurry's material removal ability. SPION adsorbs a more significant amount of –OH groups at a higher pH than a slurry with a lower pH value and it confirmed from the FTIR spectrum in Fig. 4c. Thus, higher pH contained slurry provides more surface finishing than the lower one via CMP process.

7. Conclusions

This study has successfully developed a Malic acid-functionalized SPION nanocomposites-based nanoabrasives via a simple chemical route. Significant effects of functionalization of SPION particles with the surface modifier on the structural, chemical, and polishing properties are investigated. The functionalized nanoabrasives were observed as spherical in shape with a narrow particle size distribution. The high surface area and dispersion properties were evaluated. The functionalization of SPION with the surface modifier does not hinder the superparamagnetic nature of the nanoabrasive however, reduced the overall magnetization value of the nanocomposite.

The following conclusions are derived from the polishing performance of the Malic acid-functionalized SPION nanocomposite-based nanoabrasives.

- Large surface area, narrow particle size distribution, and homogeneous particle stacking of the functionalized nanoabrasive increases the contact area (in terms of surface to volume ratio) between the glass surface and the polishing abrasive. These aid in the mechanical action of the CMP in attaining uniform nanometric cutting effect of the glass specimen.
- The domain of colloidal science and analytical tools helped to characterize the chemical processes and the surface chemistry between nanoabrasive particles and the top-most atomic layers of optical glasses in precision optical polishing. This allowed us to systematically investigate the limitation of the bare-SPION particles and the strength of the functionalized SPION-based nanoabrasive.
- The pivotal role of the surface charge of outer surface of the functionalized nanoabrasive, and pH of the slurry kept in maintaining favourable conditions for a well-dispersed polishing.
- The Malic acid-functionalized based nanoabrasive provides much reduced surface roughness of 0.23 nm in the case of BK7 glass and 0.1 nm for fused silica glass.
- The polishing results indicated that the surface finishing for superfinish polishing depends on the type of surface modifier is used, the surface area of the resultant nanoabrasive, their particle size distribution of the nanoabrasives, the pH of the slurry, and the surface charge of the outer surface of the nanoabrasive particles.

8. Data availability statement

All relevant data are included in the figures and tables in the

manuscript and in the supplementary information file. Additional data (if any) are available from the authors upon reasonable request.

Declaration of Competing Interest

The authors declare that they have no known competing financial interests or personal relationships that could have appeared to influence the work reported in this paper.

Data availability

The authors do not have permission to share data.

Appendix A. Supplementary material

Supplementary data to this article can be found online at https://doi.org/10.1016/j.optlastec.2023.109191.

References

[1] M.J. Di Pirro, P. Shirron, M. Kimball, J. Tuttle, A. Jahromi, D. Glaister, J. Olson, M. Petach, M. Zagarola, Cryocooling technologies for the Origins Space Telescope, J. Astron. Telesco. Instrum. Syst. 7 (1) (2021), 011008.

[2] D. Vukobratovich, J.P. Schaefer, Large stable aluminum optics for aerospace applications, Proc. SPIE, Optomechanics 2011: Innovations and Solutions, 8125 (2011) 81250T.

[3] J.E. Harvey, K.L. Lewotsky, A. Kotha, Effects of surface scatter on the optical performance of x-ray synchrotron beam-line mirrors, Appl. Opt. 34 (1995) 3024–3032.

[4] Q. Lin, K. Cai, R. Yang, et al., Geometric calibration of markerless optical surgical navigation system, Int. J. Med. Robotics Comput. Assist. Surg. 5 (2019) e1978.

[5] R.H. Stulen, D.W. Sweeney, Extreme ultraviolet lithography, IEEE J. Quantum Electron. 35 (5) (1999) 694–699.

[6] E. Ignesti, F. Tommasi, L. Fini, F. Martelli, N. Azzali, S. Cavalieri, A new class of optical sensors: a random laser-based device, Sci Rep. 6 (2016) 35225.

[7] J.K. Lawson, D.M. Aikens, R.E. English Jr. C.R. Wolfe, Power spectral density specifications for high-power laser systems, in: Proc. SPIE, Specification, Production, and Testing of Optical Components and Systems, 2775, 1996.

[8] P.B. Zantyea, A. Kumar, A.K. Sikder, Chemical mechanical planarization for microelectronics applications, Mat. Sci. Eng. Res. 45 (3) (2004) 89–220.

[9] G.S. Khan, M. Gubarev, C. Speegle, B. Ramsey, Computer-Controlled Cylindrical Polishing Process for Large X-Ray Mirror Mandrels, Proc SPIE 7802 (2010).

[10] G.S. Khan, M. Gubarev, C. Speegle, B. Ramsey, Deterministic Computer-Controlled Polishing Process for High-Energy X-Ray Optics, in Optical Fabrication and Testing, OSA Technical Digest (CD) (2010), paper OThB2.

[11] R. Graue, G. Valsecchi, "Superfinish technology for enhanced grazing incidence reflectivity in x-ray telescopes," Proc. SPIE 2805, Multilayer and Grazing Incidence X-Ray/EUV Optics III, (1996); doi:10.1117/12.245106.

[12] L. Wang, Z. Yang, G. Li, Y. Liang, "Effect of surface roughness on the measurement of high-power laser with a cone-shaped cavity, in: Proc. SPIE 6150, 2nd International Symposium on Advanced Optical Manufacturing and Testing Technologies: Optical Test and Measurement Technology and Equipment, 615006 (2006); doi: 10.1117/12.676426.

[13] W.I. Kordonski, Magnetorheological finishing, Int. J. Mod. Phys. B. 10 (23/24) (1996) 2837–12284.

[14] A.K. Singh, S. Jha, P.M. Pandey, Mechanism of material removal in ball end magnetorheological finishing process, Wear 302 (1–2) (2013) 1180–1191.

[15] M.R. Sankar, V.K. Jain, J. Ramkumar, Rotational abrasive flow finishing (R-AFF) process and its effects on finished surface topography, Int. J. Mach. Tools Manuf. 50 (7) (2010) 637–650.

[16] K. Naveen, V.V. Shanbhag, N. Balashanmugam, P. Vinod, Ultra-precision finishing by magnetic abrasive finishing process, Mater. Today: Proc. 5 (5) (2018) 12426–12436.

[17] S. Jha, V.K. Jain, Design and development of the magnetorheological abrasive flow finishing (MRAFF) process, Int. J. Mach. Tools Manuf. 44 (10) (2004) 1019–1029.

[18] Y. Mori, K. Yamauchi, K. Endo, Elastic emission machining, Precis. Eng. 9 (3) (1987) 123–128.

[19] N. Umehara, T. Kirtane, R. Gerlick, V.K. Jain, R. Komanduri, A new apparatus for finishing large size/large batch silicon nitride (Si_3N_4) balls for hybrid bearing applications by magnetic float polishing (MFP), Int. J. Mach. Tools Manuf. 46 (2) (2006) 151–169.

[20] D. Zhao, X. Lu, Chemical mechanical polishing: Theory and experiment, Friction 1 (2013) 306–326.

[21] N. Belkhir, D. Bouzid, V. Herold, Morphological behavior and wear of polyurethane pads used in glass polishing process, Precis. Eng. 36 (4) (2012) 641–649.

[22] V.K. Jain, Magnetic field assisted abrasive based micro-/nano-finishing, J. Mater. Process. Technol. 209 (2009) 6022–6038.

[23] Y. Xie, B. Bhushan, Effects of particle size, polishing pad and contact pressure in free abrasive polishing, Wear 200 (1996) 281–295.

[24] M.J. Cumbo, D. Fairhurst, S.D. Jacobs, B.E. Puchebner, Slurry particle size evolution during the polishing of optical glass, Appl. Opt. 34 (19) (1995) 3743–3755.

[25] H. Lei, Q. Gu, R. Chen, Z. Wang, Preparation of Fe-doped colloidal SiO_2 abrasives and their chemical mechanical polishing behavior on sapphire substrates, Appl. Opt. 54 (24) (2015) 7188–7194.

[26] G. Zhao, Z. Wei, W. Wang, D. Feng, A. X, W. Liu, Z. Song, Review on modeling and application of chemical mechanical polishing, Nanotechnol. Rev. 9 (2020) 182–189.

[27] X. Chen, Y. Zhao, Y. Wang, Modeling the effects of particle deformation in chemical mechanical polishing, Appl. Surf. Sci. 258 (2012) 8469–8474.

[28] M. Amir, V. Mishra, R. Sharma, S.W. Ali, G.S. Khan, Polishing Performance of Magnetic Nanoparticles based Nanoabrasive for Superfinish Optical Surface, Appl. Opt. 61 (2022) 5179–5188.

[29] M. Amir, V. Mishra, R. Sharma, S.W. Ali, G.S. Khan, Polishing prformance of recyclable and reusable SiO_2 magnetic nanoparticle-based polishing-abrasive, Mater. Today: Proc. 60 (2022) 773–776.

[30] M. Amir, U. Kurtan, A. Baykal, Synthesis and application of magnetically recyclable nanocatalyst Fe_3O_4@Nico@Cu in the reduction of azo dyes, Chinese, J. Catal. 36 (2015) 1280–1286.

[31] D. Speed, P. Westerhoff, R. Sierra-Alvarez, R. Draper, P. Pantano, S. Aravamudhan, K.L. Chen, K. Hristovski, P. Herckes, X. Bi, Y. Yang, C. Zeng, L. Otero-Gonzalez, C. Mikoryak, B.A. Wilson, K. Kosaraju, M. Tarannum, S. Crawford, P. Yi, X. Liu, S. V. Babu, M. Moinpour, J. Ranville, M. Montano, C. Corredor, J. Posner, F. Shadman, Physical, chemical, and in vitro toxicological characterization of nanoparticles in chemical mechanical planarization suspensions used in the semiconductor industry: towards environmental health and safety assessments, Environ. Sci. Nano. 2 (2015) 227–244.

[32] T.S. Sreeremya, M. Prabhakaran, S. Ghosh, Tailoring the surface properties of cerium oxide nanoabrasives through morphology control for glass CMP, RSC Adv. 5 (2015) 8405–84065.

[33] Z. Zhang, W. Liu, Z. Song, Particle size and surfactant effects on chemical mechanical polishing of glass using silica-based slurry, Appl. Opt. 49 (28) (2010) 5480–5485.

[34] U. Kurtan, M. Amir, A. Baykal, Fe_3O_4@Nico-Ag magnetically recyclable nanocatalyst for azo dyes reduction, Appl. Surf. Sci. 363 (2016) 66–73.

[35] M. Amir, S.W. Ali, A. Baykal, G.S. Khan, Development of highly active, chemically stable and recyclable magnetic nanophotocatalyst based on plasmonic silver nanoparticles and photosensitive trans-3-(trans-4-imidazolyl) acrylic acid molecules, Appl. Organomet. Chem. 35 (6) (2021) e6229.

[36] M.A. Abdullahi, M. Amir, S.M. Asiri, A.D. Korkmaz, A. Baykal, G.S.P. Soylu, S. Karakuş, A. Kilislioğlu, Photocatalytic degradation of azo dyes and organic contaminants in wastewater using magnetically recyclable Fe_3O_4@UA-Cu Nano-Catalyst, Catal. Lett. 148 (4) (2018) 1130–1141.

[37] M. Amir, S. Güner, A. Yildiz, A. Baykal, Magneto-optical and catalytic properties of Fe_3O_4@HA@Ag magnetic nanocomposite, J. Magn. Magn. Mater. 421 (2017) 462–471.

[38] P. Mukherjee, A. Ahmad, D. Mandal, S. Senapati, S.R. Sainkar, M.I. Khan, R. Parishcha, P.V. Ajaykumar, M. Alam, R. Kumar, M. Sastry, Fungus-mediated synthesis of silver nanoparticles and their immobilization in the mycelial matrix: a novel biological approach to nanoparticle synthesis, Nano Lett. 1 (2001) 515–519.

[39] M. Focsan, A.M. Gabudean, V. Canpean, D. Maniu, S. Astilean, Formation of size and shape tunable gold nanoparticles in solution by bio-assisted synthesis with bovine serum albumin in native and denatured state, Mater. Chem. Phys. 129 (2011) 939–942.

[40] M. Shahriarya, H. Veisib, M. Hekmatia, S. Hemmati, In situ green synthesis of Ag nanoparticles on herbal tea extract (Stachys lavandulifolia)-modified magnetic iron oxide nanoparticles as antibacterial agent and their 4-nitrophenol catalytic reduction activity, Mater. Sci. Eng. C. 90 (2018) 57–66.

[41] M. Amir, H. Sözeri, A.D. Korkmaz, A. Baykal, Concentration and temperature-dependent magnetic properties of $Ba_{1-x}Zn_xFe_{12}O_{19}$ hexaferrites, Ceram. Inter. 44 (2018) 988–992.

[42] R. Day, M. Fuller, V.A. Schmidt, Hysteresis properties of titanomagnetites: grain-size and compositional dependence, Phys. Earth Planet. Inter. 13 (4) (1977) 260–267.

[43] W.M. Daoush, Co-precipitation and magnetic properties of magnetite nanoparticles for potential biomedical applications, J. Nanomed. Res. 5 (2017) 1–6.

[44] D. Chicot, J. Mendoza, A. Zaoui, G. Louis, V. Lepingle, F. Roudet, J. Lesage, Mechanical properties of magnetite (Fe_3O_4), hematite (alpha-Fe_2O_3) and goethite (alpha-FeO·OH) by instrumented indentation and molecular dynamics analysis, Mater. Chem. Phys. 129 (2011) 862–870.

[45] A.H. Yusoff, M.N. Salimi, M.F. Jamlos, A review: Synthetic strategy control of magnetite nanoparticles production, Adv. Nano Res. 6 (1) (2018) 1–19.

[46] A. Baykal, M. Amir, S. Güner, H. Sözeri, Preparation and characterization of SPION functionalized via caffeic acid, J. Magn. Magn. Mater. 395 (2015) 199–204.

[47] J.M.D. Coey, Noncollinear spin arrangement in ultrafine ferrimagnetic crystallites, Phys. Rev. Lett. 27 (1971) 1140.

[48] C. Liu, B. Zou, A.J. Rondinone, Z.J. Zhang, Chemical control of superparamagnetic properties of magnesium and cobalt spinel ferrite nanoparticles through atomic level magnetic couplings, J. Am. Chem. Soc. 122 (26) (2000) 6263–6267.

[49] M. Hu, H.-J. Butt, K. Landfester, M.B. Bannwarth, S. Wooh, H. Thérien-Aubin, Shaping the assembly of superparamagnetic nanoparticles, ACS Nano 13 (3) (2019) 3015–3022.

[50] E. Tombácz, pH-dependent surface charging of metal oxides, Chem. Eng. 53 (2) (2009) 77–86.

[51] S. Mustafa, B. Dilara, A. Naeem, N. Rahana, P. Shahida, Sorption of metal ions on a mixed oxide [0.5M SiO_2: 0.5 M Fe(O_H)3], Adsorpt. Sci. Technol. 20 (3) (2002) 215–230.

[52] S. Liang, X. Jiao, X. Tan, J. Zhu, Effect of solvent film and zeta potential on interfacial interactions during optical glass polishing, Appl. Opt. 57 (20) (2018) 5657–5665.

[53] G. Chen, Z. Ni, Y. Bai, Q. Li, Y. Zhao, The role of interactions between abrasive particles and the substrate surface in chemical-mechanical planarization of Si-face 6H-SiC, RSC Adv. 7 (2017) 16938–16952.

[54] T. Gopal, J.B. Talbot, Effects of CMP slurry chemistry on the zeta potential of alumina abrasives, J. Electrochem. Soc. 153 (7) (2006) G622–G625.

[55] S. Sundararajan, D.G. Thakurta, D.W. Schwendeman, S.P. Murarka, W.N. Gill, Two-dimensional wafer-scale chemical mechanical planarization models based on lubrication theory and mass transport, J. Electrochem. Soc. 146 (1999) 761–766.

[56] C-W. Liu, B.-T. Dai, W.-T. Tseng, C.-F. Yeh, Modeling of the wear mechanism during chemical-mechanical polishing, J. Electrochem. Soc. 143 (1996) 716-721.

[57] S.R. Runnel, L.M. Eyman, Tribology analysis of chemical-mechanical polishing, J. Electrochem. Soc. 141 (1994) 1698–1701.

[58] T.-K. Yu, C.C. Yu, M. Orlowski, A Statistical Polishing Pad Model for Chemical-Mechanical Polishing, in: Proc. 1993 IEEE Int. Electron Dev. Mfg., 1993, pp. 865-868.

[59] N.J. Brown, P.C. Baker, R.T. Maney, Optical polishing of metals, Proc. SPIE 306 (1981) 42–57.

[60] M. Bielmann, U. Mahajan, R.K. Singh, Effect of particle size during tungsten chemical mechanical polishing, Electrochem. Solid State Lett. 2 (2009) 401–403.

[61] T. Suratwala, M. Feit, W. Steele, L. Wong, N. Shen, R. Dylla-Spears, R. Desjardin, D. Mason, P. Geraghty, P. Miller, S. Baxamusa, Microscopic removal function and the relationship between slurry particle size distribution and workpiece roughness during pad polishing, J. Am. Ceram. Soc. 97 (1) (2014) 81–91.

[62] L.M. Cook, Chemical processes in glass polishing, J. Non. Cryst. Solids. 120 (1990) 152–171.

[63] R. Iler, The chemistry of silica, Wiley, New York, 1979.

[64] J. Luo, D.A. Dornfeld, Material removal mechanism in chemical mechanical polishing: theory and modeling, IEEE Trans. Semiconductor Manuf. 14 (2) (2001) 112–133.

[65] L. Holland, The properties of glass surfaces, Chapman and Hall, London, 1964.